CHAPTER IV

Effect of Ca Doping at Bi-site on the Conductivity of $Bi_4V_2O_{11}$

The important thing in science is not so much to obtain new facts as to discover new ways of thinking about them.

Sir William Bragg

4.1. Introduction

A substantial amount of work has been carried out on V-site substitution of $Bi_4V_2O_{11}$. The aliovalent metal ions such as Cu, Co, Ni, Ti, Zn, etc. on V-site substitution of $Bi_4V_2O_{11}$ have been found most suitable in enhancing oxygen ion conductivity [**1-3**] in the intermediate temperature range. On the other hand, only scanty reports are available for substitution at Bi-site of $Bi_4V_2O_{11}$ [**4-5**]**.** Like other aliovalent compounds, works on substitution of V by Ca (BICAVOX system) have been carried out [**5-6**], but no study pertaining to Ca doping at Bi-site exists however. The introduction of Ca into V-site successfully stabilizes the tetragonal γ-phase of $Bi_4V_2O_{11}$ at room temperature for Ca amount $\geq$ 0.13 and enhancement of ionic conductivity in comparison to the parent compound [**6**] has been observed in the substitutional range mentioned earlier. On the other hand, the phase diagram study for the compositional range of BICAVOX systems reveals that the substitution mechanism for Ca doping compositions corresponds to Bi $\rightarrow$ Ca [**5**]. This also seems to be more convincing due to closer ionic radii of Ca^{2+} (99 pm) and Bi^{3+} (103 pm) [**5-7**] as compared to very small ionic radius of V^{5+} (59 pm). Hence, it seems interesting to study the effect of Ca substitution at Bi-site on the ionic conductivity of BIMEVOX.

This chapter describes a systematic study of the pure compound $Bi_4V_2O_{11}$and influence of partial substitution of Ca at Bi-site on the phase transition and electrical conductivity of $Bi_4V_2O_{11-\delta}$ solid electrolyte which can be formulated as $Bi_{4-x}Ca_xV_2O_{11-\delta}$; $0 \leq x \leq 0.4$.

4.2. Experimental

The solid solution for $Bi_{4-x}Ca_xV_2O_{11-\delta}$ ($0 \leq x \leq 0.4$) were prepared by conventional solid state reaction technique by taking stoichiometric amounts of Bi_2O_3 (99%), V_2O_5 (99%) and $CaCO_3$ (98.5%). The details of the experimental techniques adopted for preparation of the samples have been discussed in **chapter-II**.

4.3. Results and discussion

4.3.1. X-ray diffraction

The room temperature XRD patterns for both doped and the undoped compounds are shown in the **Fig.4.1**. It has been observed that the compositions $0 \leq x \leq 0.3$ show α-phase of orthorhombic structure distinguished by the characteristic doublet at $2\theta \approx 32°$ ascribed to (020) and (200) reflections [**8**]. Moreover, it has also been observed that the compositions show doublets at 39°, 48°, 54° and a weak reflection at $2\theta \approx 24°$.

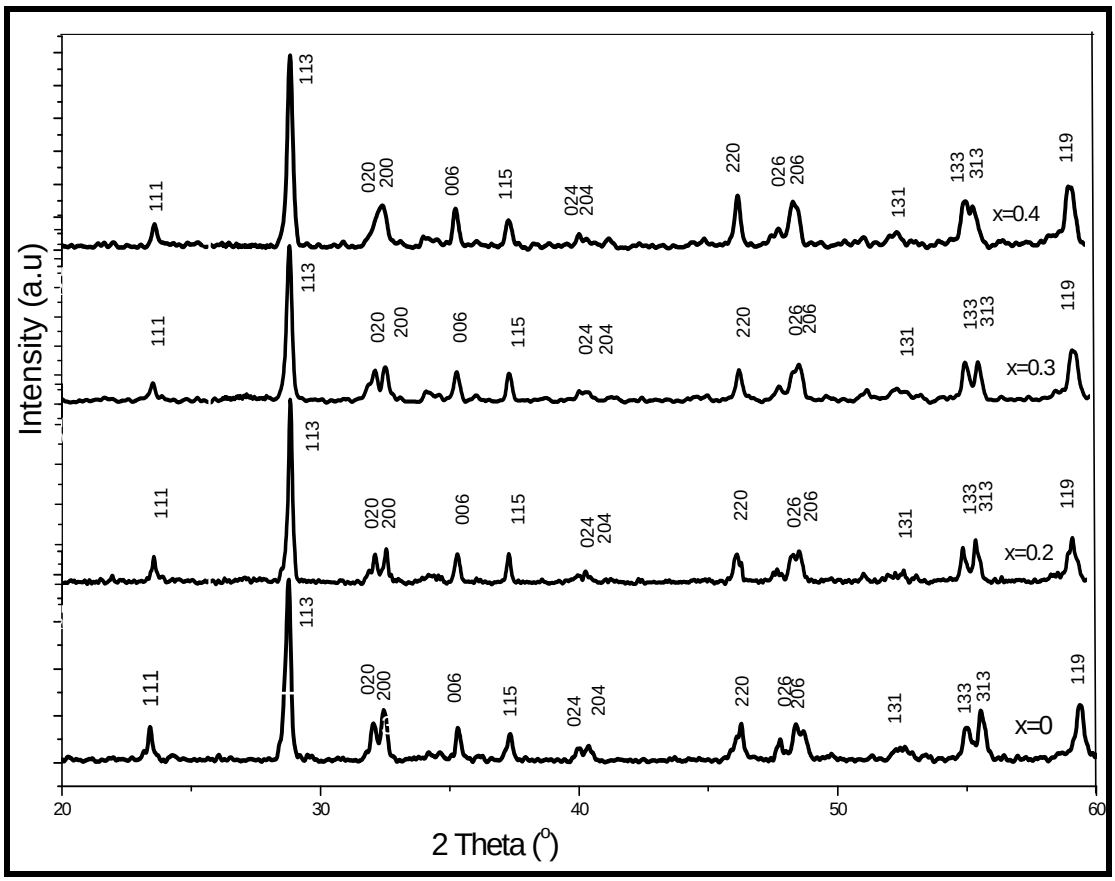

Fig. 4.1: XRD patterns of $Bi_{4-x}Ca_xV_2O_{11-\delta}$ series of compounds.

This weak reflection indicates the presence α-phase of the parent compound $Bi_4V_2O_{11}$ [**9-10**]. The monoclinic α-phase is characterized by the occurrence of doublet between 45.5° and 46.5° which is a singlet in orthorhombic structure. As shown in **Fig.4.1,** this doublet for the compositions $0 \leq x \leq 0.3$ converged to a singlet ascribed to (220) reflection which confirms the presence of orthorhombic structure [**6, 9-10**].

On the other hand for x = 0.4, the splitting at about 32° (corresponding to 020 and 200 reflections) begun to converge and transform to a peak broadening effect indicating room temperature stabilization of γ-polymorph at room temperature. Similar features have been reported for BINIVOX system [**11**].

The analysis of XRD diffratograms have been carried out in accordance to what has been described in Chapter III. The calculation of lattice parameters were performed keeping in mind good conformity between the observed and calculated values of inter-planer spacing 'd'. The indexing of XRD reflections by POWD MULT program for some representative specimens (parent, high conducting and low conducting samples) are shown in **Table 4.1 (a-c)**.

Table 4.1(a-c): The indexing of XRD reflections by POWD MULT program.

(a) Compound $Bi_4V_2O_{11}$

Sys. ORTH. Lambda = 1.541800, S.D. = 0.02001A

a = 5.521 Å, b = 5.598 Å, c = 15.243 Å,

Sl. No.	d-spacing A.		Indices			2Theta Deg.	
	obs.	calc.	h	k	l	obs.	calc.
1	3.8601	3.860	0	0	4	23.04	23.04
2	3.1426	3.1412	1	1	3	28.40	28.41
3	2.8278	2.8159	0	2	0*	31.64	31.78
4	2.7866	2.7702	0	2	1	32.12	32.31
5	2.5722	2.5739	0	0	6	34.88	34.86
6	2.4372	2.4366	1	1	5	36.88	36.89
7	2.2561	2.2497	2	1	3*	39.96	40.08
8	1.8924	1.8923	2	0	6	48.08	48.08
9	1.8879	1.8773	0	3	0	48.20	48.49
10	1.6797	1.6764	3	0	4*	54.64	54.75
11	1.6662	1.6684	2	2	5*	55.12	55.04
12	1.6628	1.6583	1	2	7	55.24	55.40

(b) Compound $Bi_{3.8}Ca_{0.2}V_2O_{11-\delta}$

Sys. ORTH. Lambda = 1.541800

a = 5.536 Å, b = 5.587 Å, c = 15.258 Å, V= 471.924 $Å^3$

Sl. No.	d-spacing A.		Indices			2Theta Deg.	
	obs.	calc.	h	k	l	obs.	calc.
1	7.6284	7.6228	0	0	2	11.60	11.61
2	3.8176	3.8192	1	1	1	23.30	23.29
3	3.8095	3.8114	0	0	4	23.35	23.34
4	3.8015	3.7629	0	1	3	23.40	23.64
5	3.1157	3.1162	1	1	3	28.65	28.65
6	2.8011	2.7993	0	2	0	31.95	31.97
7	2.7925	2.7799	2	0	0*	32.05	32.20
8	2.5495	2.5409	0	0	6*	35.20	35.32
9	2.4138	2.4125	1	1	5	37.25	37.27
10	2.4107	2.3757	1	2	2	37.86	37.75
11	2.2459	2.2460	2	0	4	40.15	40.15
12	2.2432	2.2434	1	2	3	40.20	40.20
13	1.9730	1.9725	2	2	0	46.00	46.01
14	1.9689	1.9562	2	2	1	46.10	46.22
15	1.8806	1.8814	0	2	6	48.40	48.38
16	1.8788	1.8755	2	0	6*	48.45	48.54
17	1.7523	1.7518	2	2	4	52.20	52.22
18	1.7510	1.7518	0	3	3	52.24	52.22
19	1.7498	1.7478	3	1	1*	52.28	52.34
20	1.6737	1.6761	0	3	4*	54.85	54.77
21	1.6709	1.6708	1	3	3	54.95	54.95
22	1.6695	1.6667	3	0	4*	55.00	55.10
23	1.6598	1.6626	3	1	3*	55.35	55.25
24	1.6557	1.6562	2	2	5	55.50	55.48

(c) Compound $Bi_{3.6}Ca_{0.4}V_2O_{11-\delta}$

Sys.ORTH. Lambda= 1.541800

a = 5.568 Å, b = 5.565 Å, c = 15.308 Å, V= 474.332 Å^3

Sl. No.	d-spacing A.		Indices			2Theta Deg.	
	obs.	calc.	h	k	l	obs.	calc.
1	7.6023	7.6002	0	0	2	11.64	11.64
2	3.8079	3.8047	1	1	1	23.36	23.38
3	3.8015	3.8001	0	0	4	23.40	23.41
4	3.7951	3.7551	0	1	3	23.44	23.69
5	3.1041	3.1052	1	1	3	28.76	28.75
6	2.7968	2.7966	0	2	0	32.00	32.00
7	2.7599	2.7612	2	0	0	32.44	32.42
8	2.7565	2.7505	0	2	1*	32.48	32.55
9	2.5411	2.5334	0	0	6*	35.32	35.43
10	2.4094	2.4045	1	1	5*	37.32	37.40
11	1.9649	1.9649	2	2	0	46.20	46.20
12	1.9633	1.9487	2	2	1	46.24	46.36
13	1.8806	1.8776	0	2	6*	48.40	48.48
14	1.6718	1.6738	0	3	4*	54.92	54.85
15	1.6684	1.6680	1	3	3	55.04	55.05
16	1.6562	1.6567	3	0	4	55.48	55.46
17	1.6540	1.6529	3	1	3	55.56	55.60
18	1.5569	1.5526	2	2	6	59.36	59.54

The composition dependence of unit cell parameters (*a*, *b*, and *c*) and volume V for the series of compound $Bi_{4-x}Ca_xV_2O_{11-\delta}$ is shown in **Table 4.2**. For undoped compound $Bi_4V_2O_{11}$, the values of the cell parameters are in good agreement with the earlier reported values [**9-10**]. The unit cell parameters (*a*, *b*, and *c*) corresponding to the compositions x < 0.4 exihibits orthorhombic superstructure [**10**] where as the composition x = 0.4 can be fitted equally to both orthorhombic and tetragonal phase (a ≈ 5.56 Å, c = 15.308 Å and volume V = 474.332 Å^3) which is most likely a sign of

stabilization of γ-phase at room temperature [**3, 13**]. It has been observed that the value of parameter *a* increases whereas *b* gradually decreases with the increasing Ca-concentration. The *c* axis dimension shows a gradual increase in size over the whole composition range and hence a gradual increase in cell volume is observed for the doped samples with respect to the parent compound. Considering that Ca^{2+} (99 pm)

Table-4.1(d) : Unit cell parameters of $Bi_{4-x}Ca_xV_2O_{11-\delta}$ series of compound.

composition	*a*(Å)	*b*(Å)	*c*(Å)	Volume(Å^3)
x = 0	5.521	5.598	15.243	471.108
x = 0.2	5.536	5.587	15.258	471.924
x = 0.3	5.558	5.574	15.282	473.441
x = 0.4	5.568	5.565	15.308	474.332

has smaller effective ionic radius than Bi^{3+}(103 pm), this finding seems contradictory. Therefore, it seems that though our aim of substitution was to introduce Ca at Bi-site, it might happens that calcium replaces V (59 pm). Like the Li-doped system (chapter III), the observed XRD pattern has got similarity with the reported XRD for V-site substitution of Ca **[6]** which further supports substitution at V-site rather than Bi site. The average crystallite size calculated from WH plot (as discussed in chapter II) shows that the crystallite size are in the nano range (43nm, 27 nm, 28 nm, and 32 nm respectively for x = 0, 0.2, 0.3 and 0.4 compositions). All the compositions show negligibly small strain values (~ 10^{-4}) which signifies that the XRD broadening is due to the nano size effect.

4.3.2. FTIR spectra

The FTIR spectra of both pure and doped compound with compositions x= 0.2 and x = 0.4 are shown in **Fig. 4.2**. It has been observed that the position of the (Bi-O) bond observed to be same for both doped and undoped compositions. On the other hand, the intensities of IR peaks corresponding to ν_s (V–O), ν_{as} (V–O) and ν_{as} (O–V–O) modes of vibration (~940 – 500 cm^{-1}) assigned to vanadate anion present in α-$Bi_4V_2O_{11}$ found to be decreases with the increase in doping concentration. These observations suggest the substitution of vanadium by calcium (as discussed in

chapter-III). Due to the increased crystallographic disordering in the perovskite vanadate layer, the fine structure in the spectra for x = 0.4 completely disappears and which in turn is indicative of the phase transition to γ-polymorph.

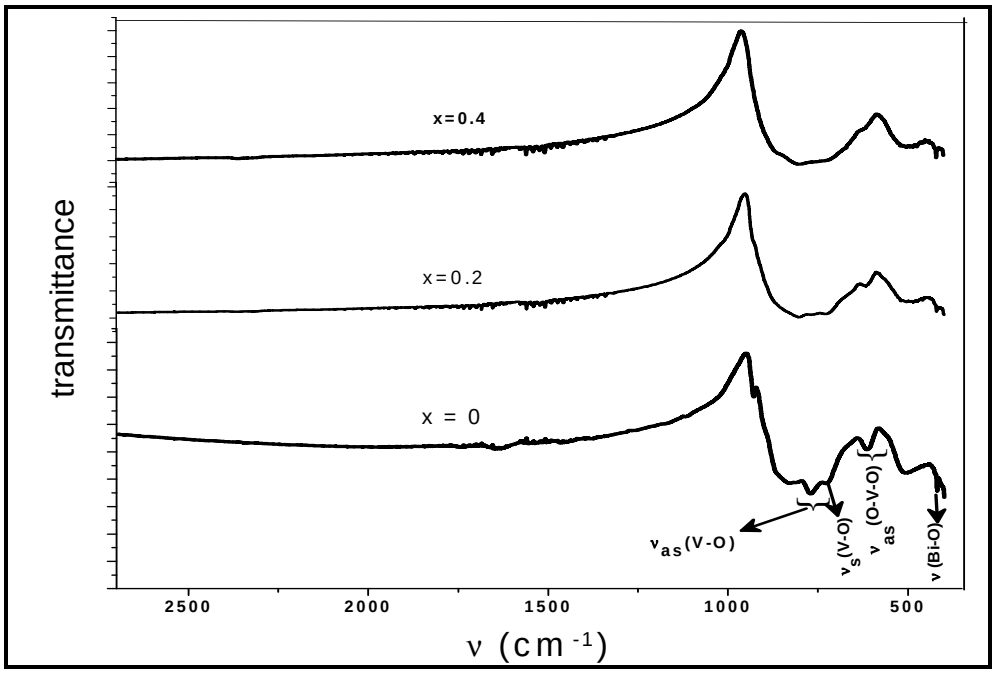

Fig.4.2: FT-IR patterns of $Bi_{4-x}Ca_xV_2O_{11-\delta}$ series of compounds.

4.3.3 Microstructure analysis

The microstructural studies on the fractured surface of the specimens are shown in **Fig. 4.3 (a-d)**. The SEM (scanning electron microscopy) of fractured surface of x = 0, x = 0.1 and x = 0.2 exhibit fairly developed grains with good grain to grain connectivity and do not show any significant change. No segregation was found to be present for the entire series (i.e., up to *x* = 0.4) of compounds suggesting that the solubility limit of Ca is more than x = 0.4 which is in agreement with the XRD results. Micro cracks within the grains have been observed in the microstructure of specimens with *x* = 0, 0.1 and 0.2. The formation of micro cracks could be ascribed to sintering at high sintering temperature (800 °C) [**14**]. The compositions *x* = 0, x = 0.1 and *x* = 0.2 do not show any significant change except some porosities in case of the sample x = 0.1 and possess almost similar grain structure with average size ~6 μm. In contrast to these, the samples with x = 0.4 composition show totally different microstructures than x = 0, x=0.1 and x = 0.2 samples, where non uniform and quite

irregular pattern is observed with average grain size ~ 4 µm. Moreover, evidence of partial melting was observed with distorted and non-uniform grain patterns and some amount of porosities were also found to be present in the micrograph of x = 0.4.

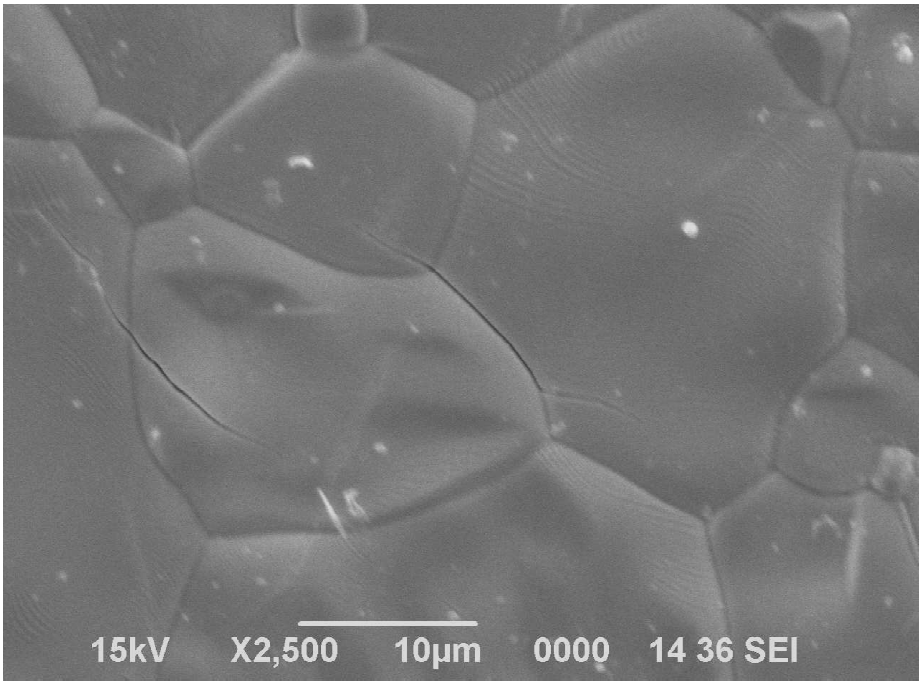

Fig. 4.3(a): SEM micrograph of x=0 specimen.

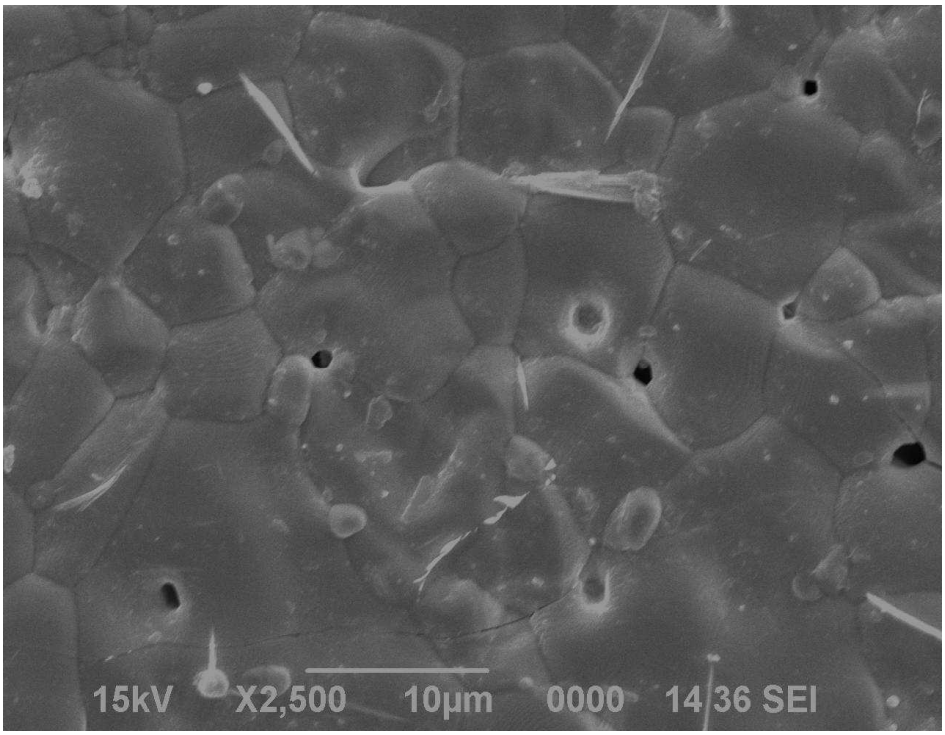

Fig. 4.3(b): SEM micrograph of x=0.1 specimen.

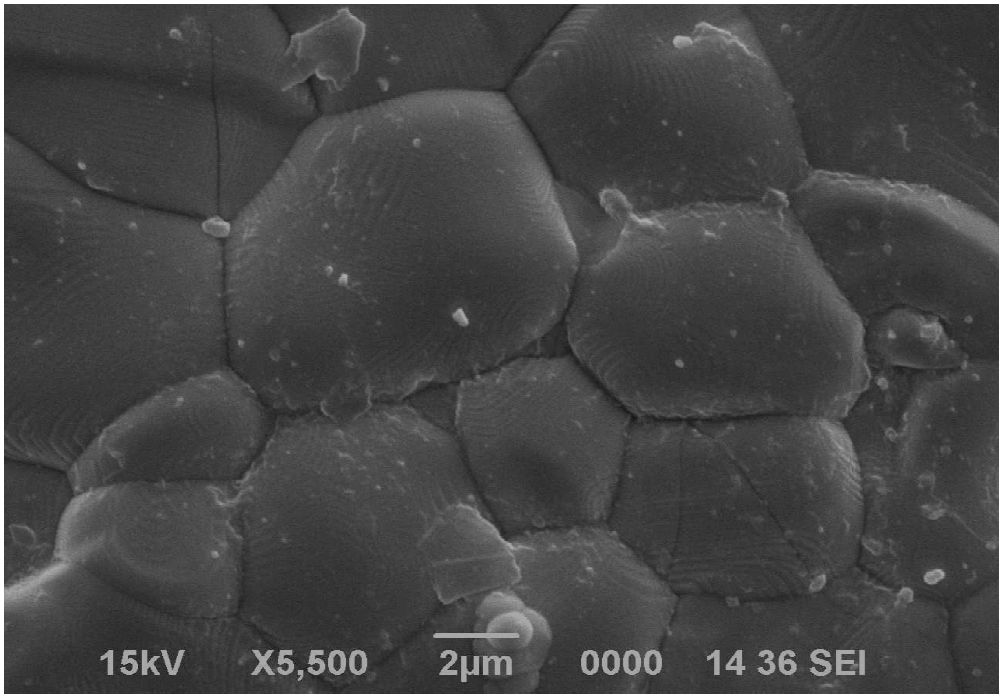

Fig. 4.3(c): SEM micrograph of x=0.2 specimen.

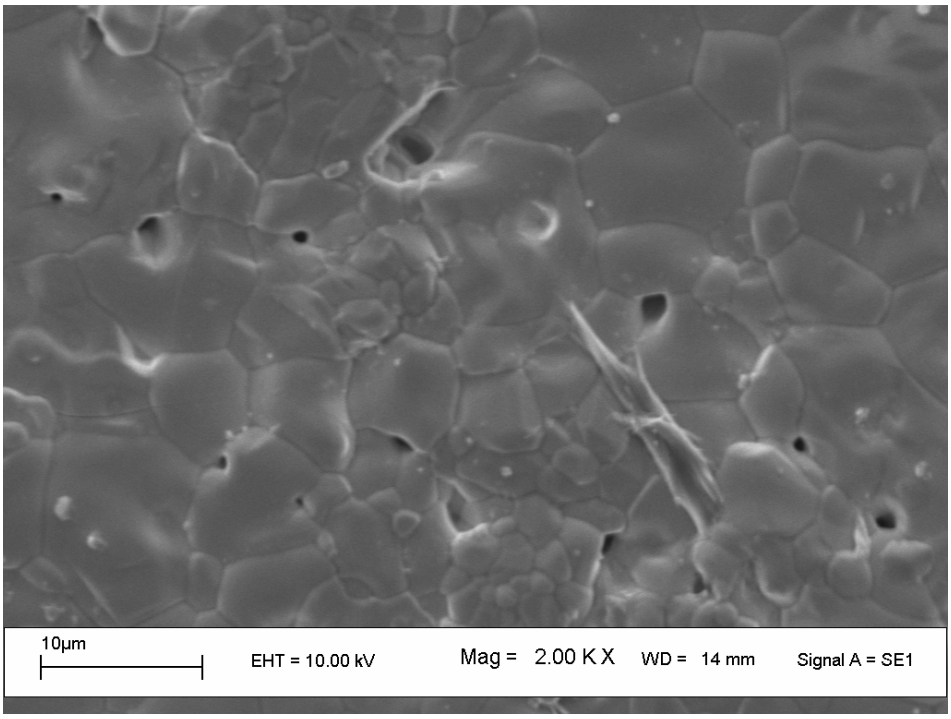

Fig. 4.3(d): SEM micrograph of x=0.4 specimen.

Partial melting of the sample may be accounted for the lowering of melting temperature with increasing Ca content. The higher ionic conductivity exhibited by the specimen x = 0.2 in $Bi_{4-x}Ca_xV_2O_{11-\delta}$ is supported by the relatively more uniformity in grains pattern and size with the absence of porosity as compared to x = 0.1 and 0.4 samples.

4.3.4. Energy dispersive X-ray spectroscopy (EDS)

Energy-dispersive X-ray spectroscopy (EDS or EDX) technique is used to determine the elemental composition of the specimens. The EDS spectra of x-ray counts vs. energy (in keV) for the specimens x = 0, x = 0.2, and x = 0.4 are shown in **Fig. 4.4**. The experimental and theoretical values of the elemental content (atomic weight percent) of different compositions have been tabulated in **Table 4.3 (a-c)**. It has been observed that the experimental values of the atomic weight percentage of elements obtained from the EDS studies are almost same with the calculated values of the respective compounds which suggest that proper stoichiometry is maintained in the compositions. To check the homogeneity of the sintered body, the pellets were broken

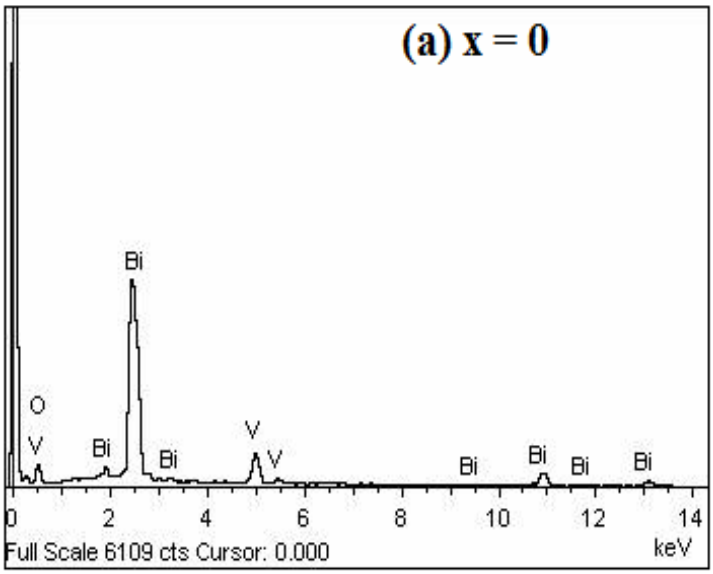

Fig. 4.4 (a): EDS spectrum of (a) *x* = 0 specimens of the series of compound $Bi_{4-x}Ca_xV_2O_{11-\delta}$.

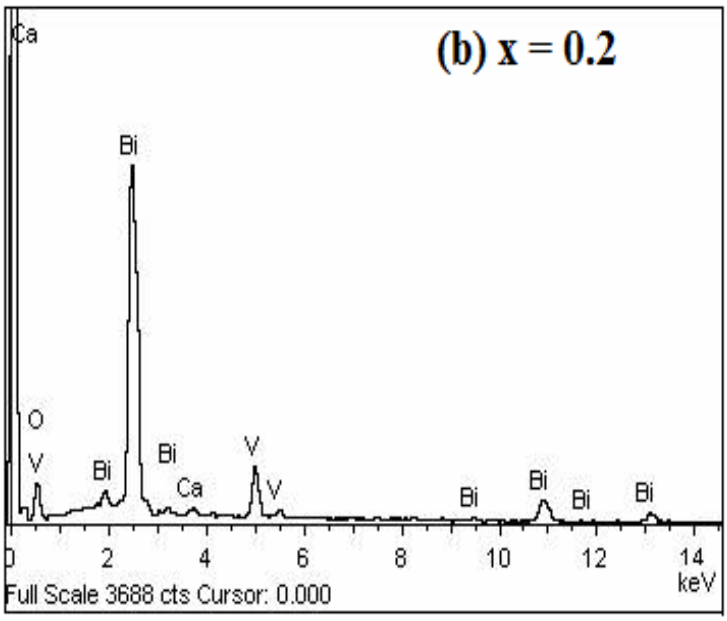

Fig. 4.4(b): EDS spectrum of (b) x = 0.2 specimens of the series of compound $Bi_{4-x}Ca_xV_2O_{11-\delta}$.

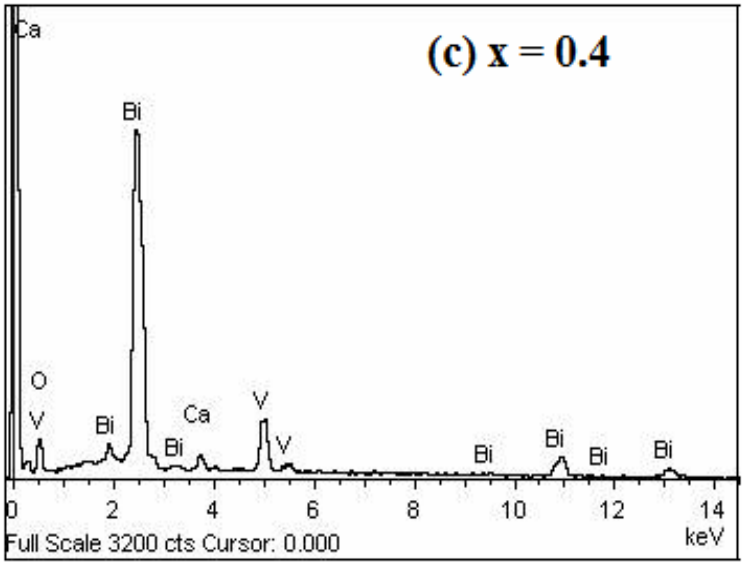

Fig. 4.4 (c): EDS spectrum of (c) x = 0.4 specimens of the series of compound $Bi_{4-x}Ca_xV_2O_{11-\delta}$.

into several pieces and EDS spectra were collected for each piece of the samples. The elemental compositions were found to be same for each sample at different inspected fields which confirms the homogeneity of the pellets.

Table 4.2 (a-c): Elemental content of different compositions of the series of compound $Bi_{4-x}Ca_xV_2O_{11-\delta}$.

(a) Elemental Content of x = 0 composition

Element	Weight% (experimental)	Weight % (theoretical)
O	15.96	15.84
V	8.98	9.17
Bi	75.06	74.98
Totals	100.00	

(b) Elemental Content of x = 0.2 composition

Element	Weight % (experimental)	Weight % (Theoretical)
O	16.37	16.17
Ca	0.84	0.74
V	9.25	9.45
Bi	73.54	73.64
Totals	100.00	

(c) Elemental Content of x = 0.4 composition

Element	Weight % (experimental)	Weight % (Theoretical)
O	16.66	16.56
Ca	1.61	1.54
V	9.38	9.77
Bi	72.35	72.13
Totals	100.00	

4.3.5 DSC studies

The DSC curves of $Bi_{4-x}Ca_xV_2O_{11-\delta}$; $0 \leq x \leq 0.4$ systems for both heating and cooling cycles are shown in **Fig. 4.5 (a-e)**. Similar to the parent compound $Bi_4V_2O_{11}$, the doped compounds show hysteresis behaviour which has been reported for other BIMEVOX compounds [**2**]. On heating, the strong endothermic peak is observed for both undoped as well as doped compound with composition $x = 0.1$ and $x = 0.2$ which clearly reveals the presence of $\alpha \rightarrow \beta$ phase transition. For the undoped compound the endothermic peak is observed at 449 °C with an enthalpy of 8.37 J/g. For the

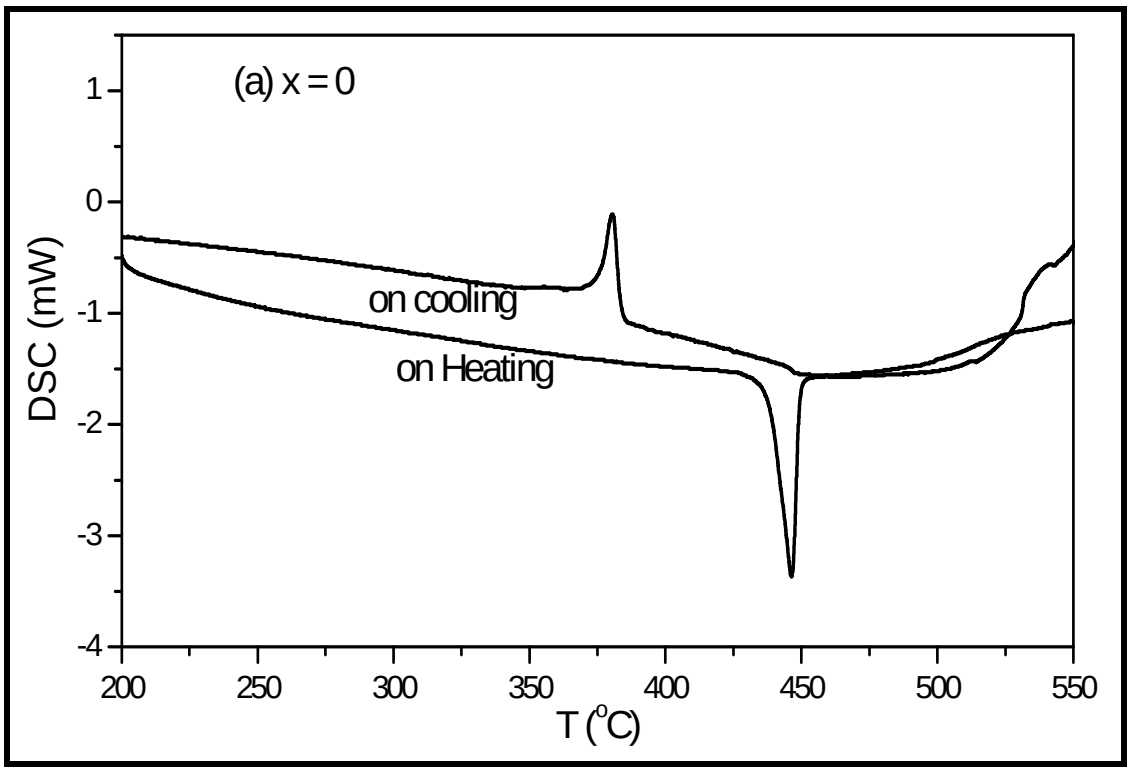

Fig. 4.5 (a): DSC plots of (a) x = 0 composition.

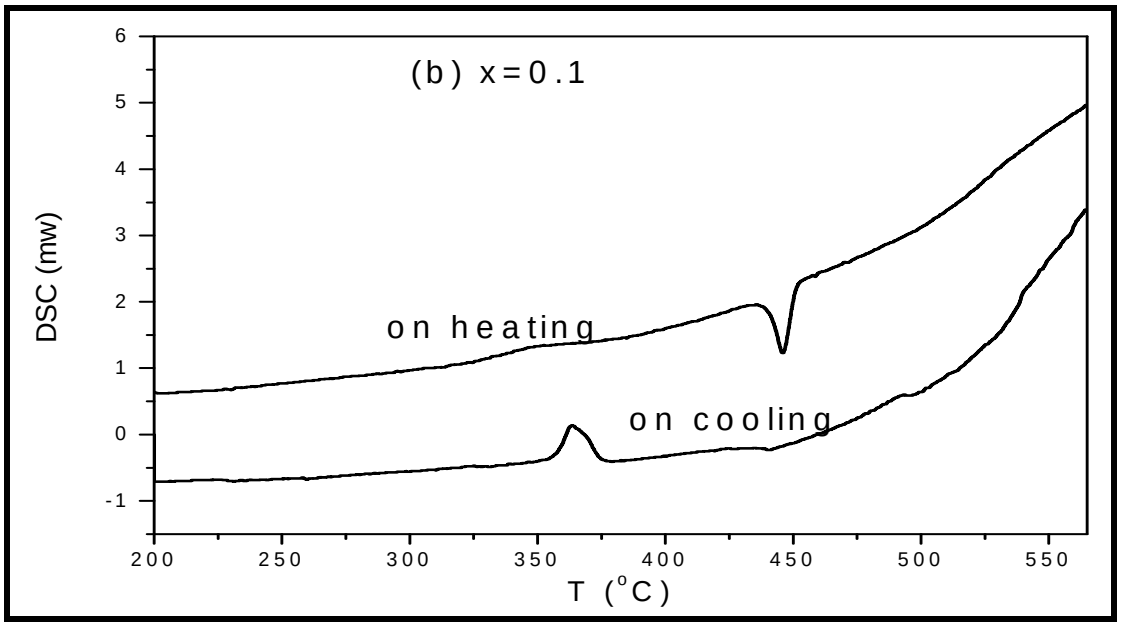

Fig. 4.5 (b): DSC plots of (b) x = 0.1 composition.

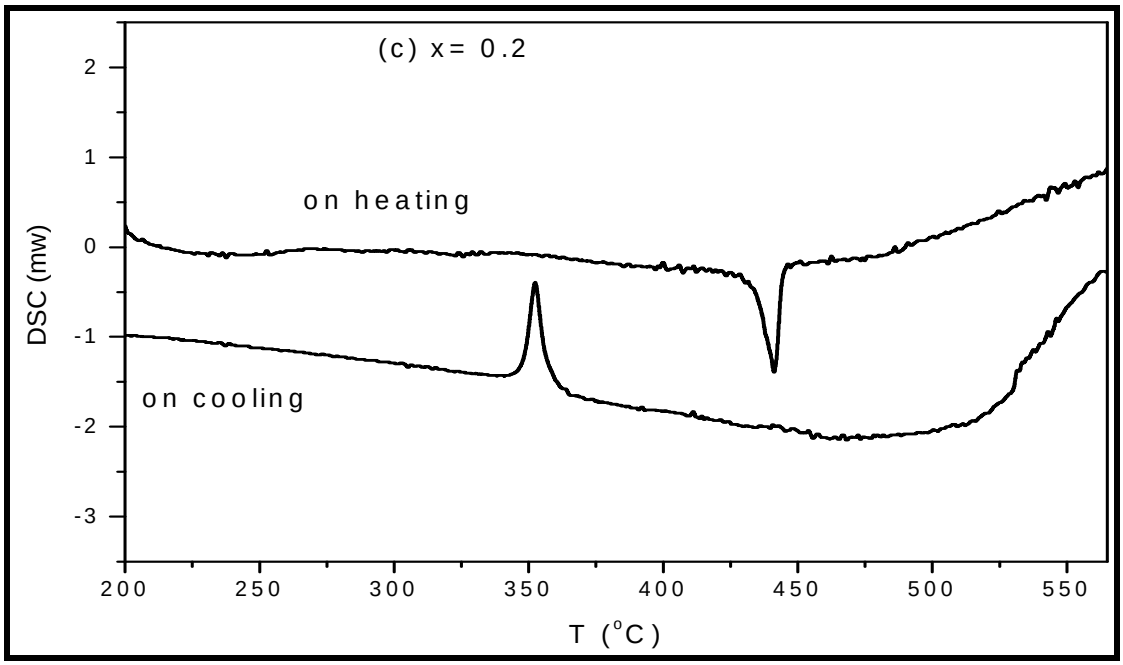

Fig. 4.5 (c): DSC plots of (c) x = 0.2 composition.

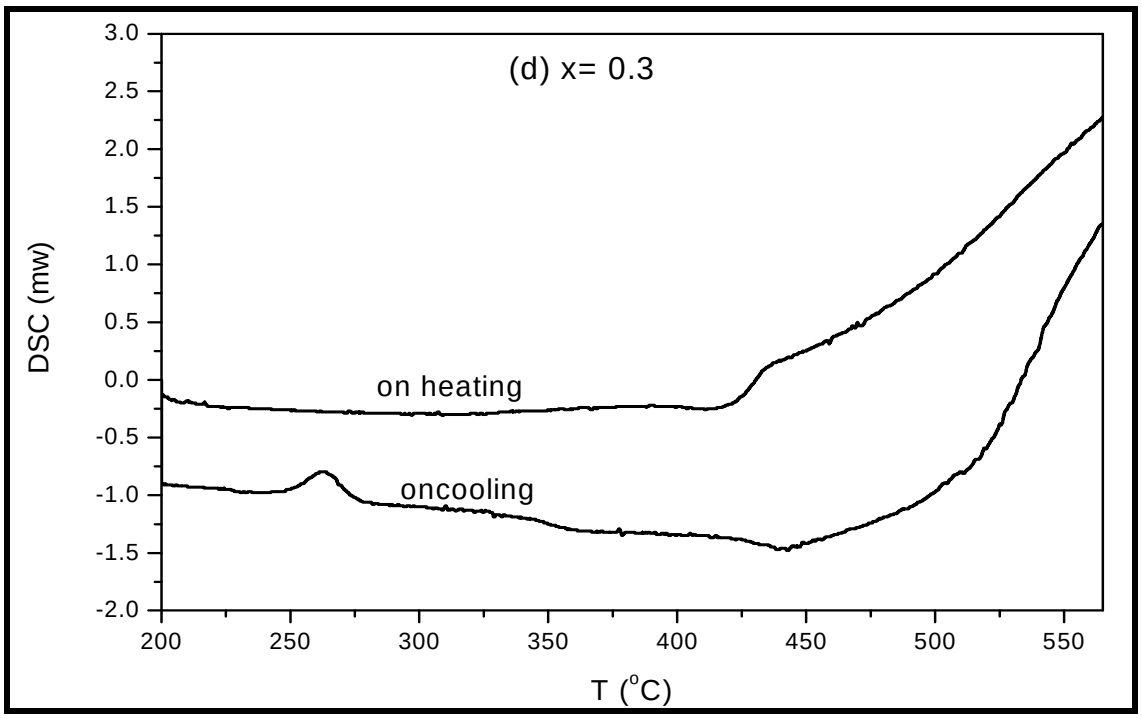

Fig. 4.5 (d): DSC plots of (d) x = 0.3 composition.

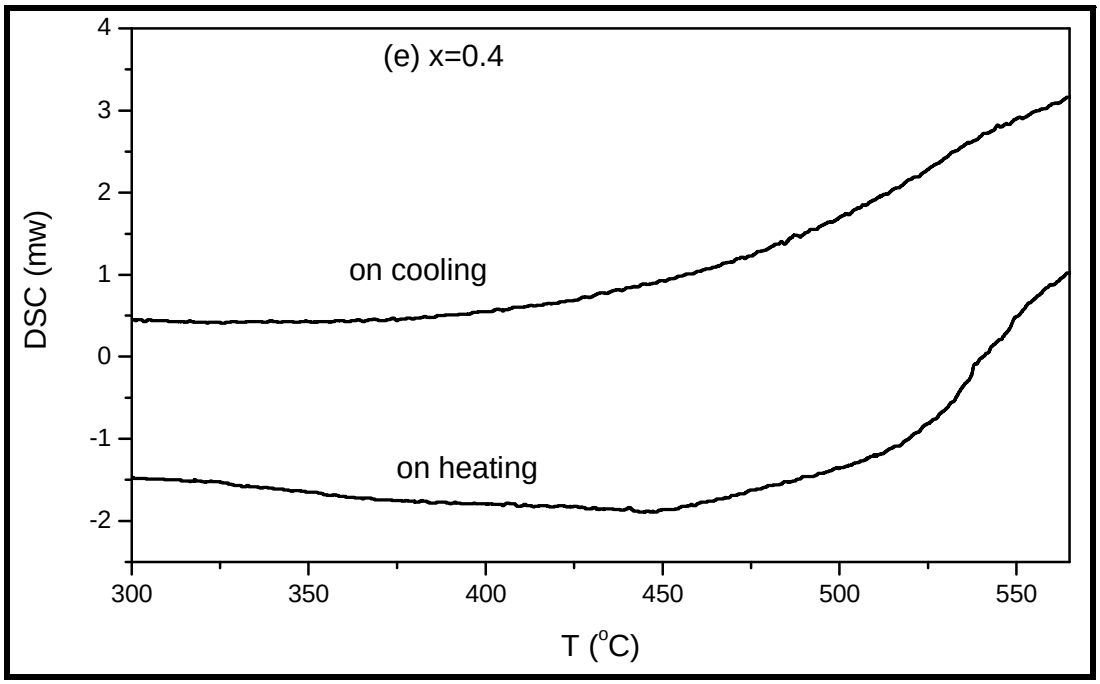

Fig. 4.5 (e): DSC plots of (e**)** x = 0.4 composition.

specimens with x = 0.1 and x = 0.2, the corresponding peaks are observed around 445 °C with enthalpy values 7.62 J/g and 6.13 J/g. For the specimen x = 0.3, the DSC peak for heating cycle further shifts towards lower temperature (417 °C) and hence indicating initiation of suppression of $\alpha \rightarrow \beta$ phase transition. Another endothermic peak is evidenced at 550 °C for the non doped compound which is an indication of $\beta \rightarrow \gamma$ transition. In cooling cycle the peaks representing $\alpha \rightarrow \beta$ phase transition shifted to 361 °C, 364 °C and 352 °C and 262 °C respectively for the specimens x = 0, x = 0.1, x = 0.2 and x = 0.3. This peak then shifts to the lower temperature, being more spread when substitution ratio increases and finally $\beta \rightarrow \gamma$ phase transition is stabilized for the compound with x = 0.4 at room temperature as no peak is observed in the either heating or cooling cycles.

4.3.6 AC impedance and conductivity analysis

In **Fig. 4.6**, impedance spectra of $Bi_{4-x}Ca_xV_2O_{11-\delta}$; $0 \leq x \leq 0.4$ series of compounds are presented at two different temperatures 300 °C (**Fig. 4.6 a-c**) and 500 °C (**Fig. 4.6 d-f**). The impedance spectra of the parent compound at 300 °C consist of two semi

circular arcs representing contributions from grain and grain boundary and an inclined spike at low frequencies. The low frequency spike is a well known feature of ionically

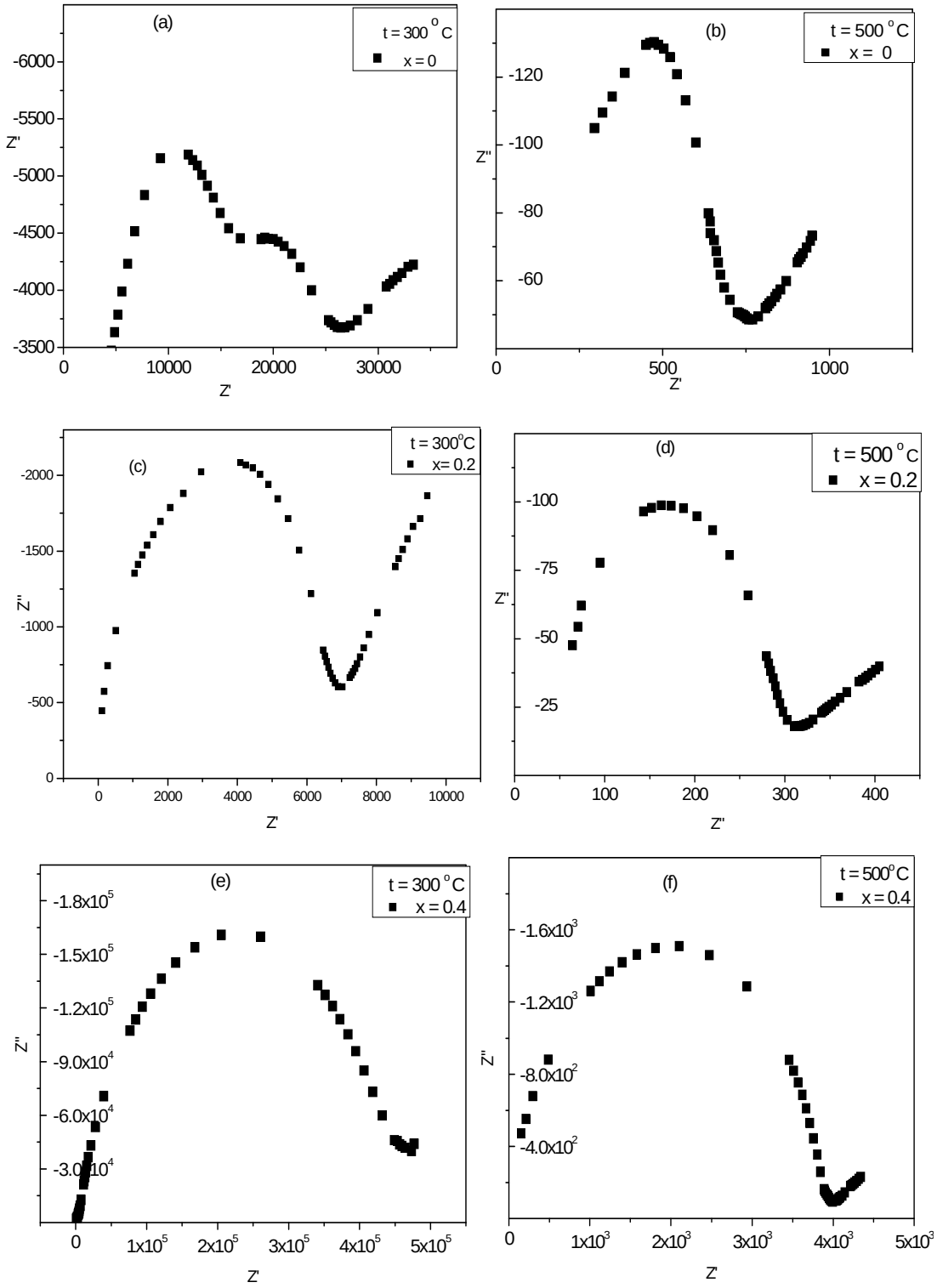

Fig. 4.6 (a-f): Impedance spectra for x=0, 0.2 and 0.4 compositions (pure, high and low conducting specimen) of $Bi_{4-x}Ca_xV_2O_{11-\delta}$ at temperatures 300 ^{0}C and 500 ^{0}C.

conducting systems [**2, 15-17**] and is attributed to the electrode polarization. On the other hand the impedance spectra for the doped samples both at 300 ^{0}C and 500 ^{0}C comprises of a single semicircular arc together with the low frequency spike. The high frequency arc has been attributed to combined effect of grain interior and the grain boundary since in the present case it is difficult to segregate effect of grain boundary and bulk contributions (except for x = 0 at 300 ^{0}C). The asymmetry in the impedance spectra presents the evidence of deviation from Debye type of relaxation process. It is evident from the impedance spectra that at the temperatures (300 ^{0}C and 500 ^{0}C), the lowest and highest bulk resistivity is observed for the specimens x = 0.2 and x = 0.4 respectively. The total resistance (grain + grain boundary) of the samples at various temperatures was determined from the intersection point of the impedance spectrum on the real axis (X-axis).

Fig. 4.7 shows the Arrhenius plots for the samples of the compound $Bi_{4-x}Ca_xV_2O_{11-\delta}$ with $0 \leq x \leq 0.4$. The compositions x = 0.1- 0.3 show three domains with different slopes suggesting the existence of $\alpha \rightarrow \beta$ (i.e., α-orthorhombic to β-orthorhombic) and $\beta \rightarrow \gamma$ (β-orthorhombic to tetragonal) phase transitions. Further, $\alpha \rightarrow \beta$ transitions seems to be partially suppressed in the composition range x = 0.1- 0.3. The degree of phase suppression increases for x = 0.4 and appears to be completely suppressed which is in conformity with DSC measurements where no phase transition was obtained for this specimen.

The conductivity behaviour of undoped and doped compounds can, in general, be divided into three regions: (a) low temperature (up to 400 °C), (b) intermediate temperature (400 °C to 500 °C), and (c) high temperature (above 500 °C). In the lower temperature regime, the conductivity of the doped compounds first increases with Ca concentration and become maximum for the composition x = 0.2 and then decreases for higher concentrations (x > 0.2). In this range of temperature, the conductivity of the compounds x $\geq$ 0.3 is less than the parent compound. In the intermediate as well as in the high temperature range, the conductivity of the specimens with x = 0.2 is significantly higher than the parent compound.

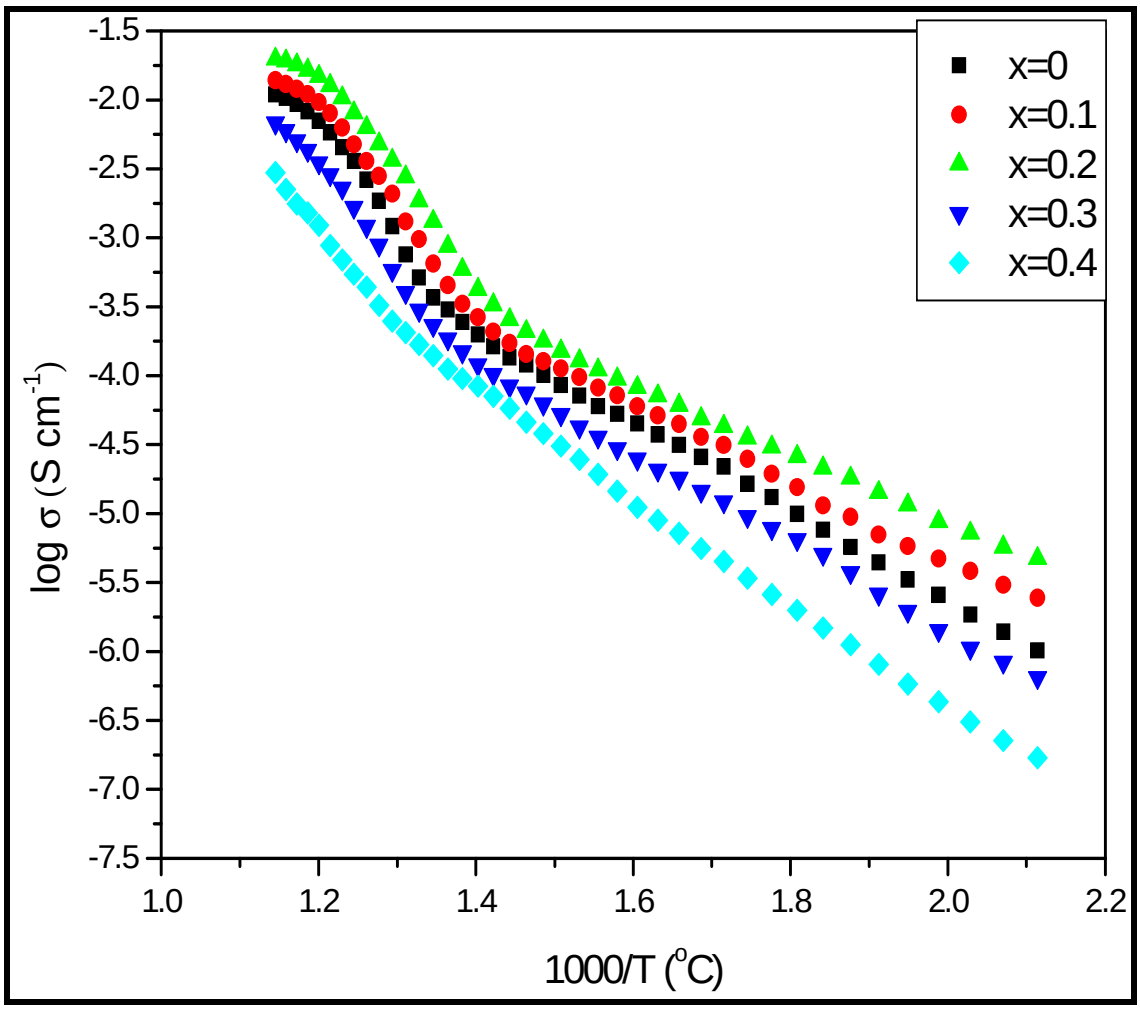

Fig. 4.7: Arrhenius plots of $Bi_{4-x}Ca_xV_2O_{11-\delta}$ ($0 \leq x \leq 0.4$) series of compounds.

It is noteworthy to mention that like the low temperature range, the conductivity plots of all the compounds maintain a similar trend in the intermediate as well as in the high temperature range. The highest conductivity (1.3×10^{-3} S/ cm^{-1}) with respect to parent compound is observed for x = 0.2 composition at 470 °C which is more than three times higher than the parent compound. The increase of ionic conductivity for the doped compounds (x = 0.1 - 0.2) as compared to the undoped one could be correlated with the increasing oxygen ion vacancies created by aliovalent substitution (Ca^{2+}) [**2, 18**]. The highest conductivity accounted for x = 0.2 substitution can be regarded as a result of optimization of oxygen vacancies and the pathways between them [**2, 18**]. On the other hand, the increase of dopant concentration induces high concentration of

defects. As a result, the defect interaction increases and may lead to a reduction in ionic conductivity corresponding to the compositions x = 0.3 and 0.4 [**19-20**].

The activation energy for the system can be calculated from dc conductivity plots (1000/T vs. logσT) with the help of the Arrhenius equation

$$\sigma = \sigma_0 \exp\left(-\frac{E_g}{KT}\right) \tag{4.1}$$

Where, K is Boltzmann constant and E_g the activation energy.

A representative plot of 1000/T vs. logσT for the calculation of activation energy below 400 °C is shown in **Fig. 4.8.**

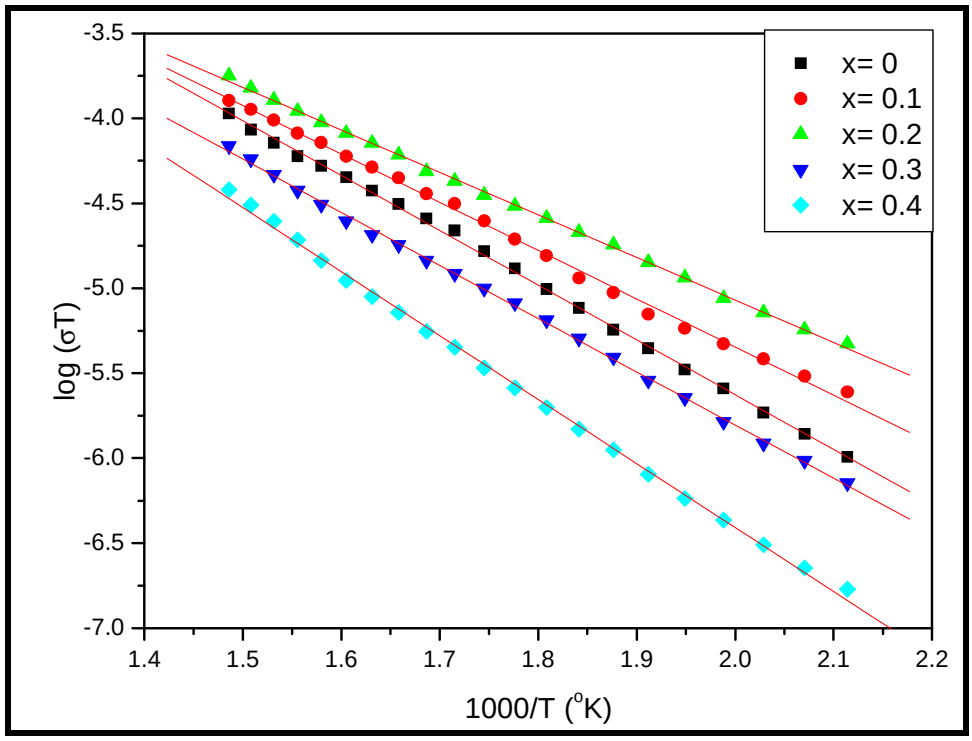

Fig.4.8: Log σT vs. 1000/T plots of $Bi_{4-x}Ca_xV_2O_{11-\delta}$ compound below 400 ^{0}C.

The value of the d.c conductivity of $Bi_{4-x}Ca_xV_2O_{11-\delta}$ series of compounds at temperatures 400 °C and 500 °C and the corresponding activation energies (below and above α → β phase transition) are shown in **Table 4.4.**

Table-4.3: Conductivity (σ) and activation energies (E_g) of $Bi_{4-x}Ca_xV_2O_{11-\delta}$ series of compounds.

Composition (x)	σ_{400} (S/cm)	σ_{500} (S/cm)	E_g (eV) (< 400°C)	E_g (eV) (> 500°C)
x = 0	1.06×10^{-4}	1.4×10^{-3}	0.63	1.25
x = 0.1	1.27×10^{-4}	2.09×10^{-3}	0.56	1.18
x = 0.2	1.77×10^{-4}	3.65×10^{-3}	0.45	1.09
x = 0.3	6.88×10^{-5}	5.8×10^{-4}	0.61	1.42
x = 0.4	3.8×10^{-5}	2.49×10^{-4}	0.74	1.50

The conductivities of the parent compound ($x = 0$) at different temperatures are close to those with previous reported studies [**15, 21**]. As observed in **Table 4.4**, the value of the activation energy in both the temperature ranges first decreases with increasing Ca content and then increases for higher doping concentration ($x \geq 0.3$). This trend of change in activation energy of the compounds is in agreement with the observed ionic conductivity.

4.4 Conclusion

1. With the introduction of Ca into $Bi_4V_2O_{11}$, the intermediate β-polymorph is partially suppressed for x=0.3 substitution and it is fully suppressed for x=0.4.

2. The FTIR studies reveal the crystallographic disturbance in the perovskite vanadate layer giving rise to phase change.

3. The SEM studies of the compositions $x = 0$, $x = 0.1$ and $x = 0.2$ show well grown grains with good grain to grain connectivity. On the other hand, non uniform and quite irregular pattern is observed for the composition x = 0.4.

4. At all temperatures the compositions with $x \leq 0.2$ possess higher ionic conductivity with respect to undoped compound.

5. The highest conductivity with respect to the parent compound is observed for x=0.2 sample with 1.3×10^{-3} S/cm^{-1} at 470 ^{0}C.

6. The increase of ionic conductivity of the doped compound as compared to the undoped compound is correlated with the increase of number of oxygen vacancies.

References

[1] M. H. Payadar, A. M. Hadian, G. Fafilek, J. Mater. Sci. **39** (2004) 1357-1361.

[2] J. Yam, M. Greenblatt, Solid State Ionics **81** (1995) 225-233.

[3] S. Beg, N. A. S. Al-Areqi, S. Haneef, Solid state Ionics **179** (2008) 2260-2264.

[4] I. Abrahams, F. Krok, Solid State Ionics **157** (2003) 139-145.

[5] C. K. Lee, G. C. Lim, A. R. West, J. Mater. Chem. **4** (1994) 1441-1444.

[6]] S. Beg, N. A. S. Al-Areqi, S. Haneef, Phase. Trans. **83** (2010) 169-181.

[7] J. A. Dean, Lange's Handbook of Chemistry, Thirteenth Edition 1985 (Mc Graw-Hill co.) 3-126.

[8] C. K. Lee, C. S. Ong, Solid State Ionics **117** (1999) 301-310.

[9] R. Kant, K. Sing, O. P. Pandey, Ionic **16** (2010) 277-282.

[10] R. Kant, K. Sing, O. P. Pandey, Ionic **15** (2009) 567-570.

[11] F. Krok, I. Abrahams, D. Bangobango, W. Bogusz, J. A. G. Nelstrop, Solid State Ionics **111**(1998) 37-43.

[12] Wu E, POWD, an interactive powder diffraction data interpretation and indexing program, version 2.5, School of Physical Sciences, Finders University of South Australia, Bedford Park, Australia.

[13] F. Krok, I. Abrahams, M. Malys, W. Bogusz, J. R. Dygas, J .A. G. Nelstrop, A. J Bush, Solid State Ionics **136-137**(2000) 119-125.

[14] C. Pirovano, M. C. Steil, E. Capoen, G. Nowogrocki, R. N. Vannier, Solid State Ionics **176** (2005) 2079-2083.

[15] R. Kant, K. Sing, O.P Pandey, Ionic **16** (2010) 277-282.

[16] J. Chmielowiec, G. Pasciak, P. Bujlo, Mater. Sci. Poland **27** (2009) 1251-1256.

[17] E. S. Buyanova, V. M. Zhukovskii, E. S. Lopatina, V. V. Ivanovskaya, E. A. Raitenko, Inorg. Mater. **38** (2002) 256-260.

[18] R. Kant, K. Sing, O. P. Pandey, Int. J. Hydrogen Energy **33** (2008) 455-462.

[19] J. A. Kilner, B. C. H. Steele, Nonstoichiometric Oxides, Academic Press Inc., NY (1981) 233-269.

[20] J. Moscinski, P. W. M. Jacobs Proceedings of the Royal Society of London. Series A, Mathematical and Physical Sciences, **398** (1985) 173.

[21] E. S. Buyanova, V. M. Zhukovskii, E. S. Lopatina, V. V. Ivanovskaya, E. A. Raitenko, Inorg. Mater. **38** (2002) 256-260.